International Global Navigation Satellite Systems Association
IGNSS Symposium 2018

Colombo Theatres, Kensington Campus, UNSW Australia
7 – 9 February 2018

Fusion of RTK GNSS receiver and IMU for accurate vehicle tracking

Shenghong Li (1)
CSIRO, Australia
(+61) 2 9372 4629 shenghong.li@csiro.au
Mark Hedley (2)
CSIRO, Australia
(+61) 2 9372 4136 mark.hedley@csiro.au
Alija, Kajan (3)
CSIRO, Australia
(+61) 2 9372 4141 alija.kajan@csiro.au
Wei Ni (4)
(+61) 2 9372 4646 wei.ni@csiro.au
Iain Collings (5)
(+61) 2 9850 9068 iain.collings@mq.edu.au

ABSTRACT

The positioning accuracy of global navigation satellite systems (GNSS) is compromised if the receiver is not in an open-sky environment. Sensor fusion is a promising technique to remedy this problem, improving the accuracy and integrity of the GNSS systems. This paper studies the fusion of Real Time Kinematic (RTK) GNSS receiver and inertial measurement unit (IMU) for accurate vehicle tracking, with a specific focus on the case where the GNSS measurements and IMU measurements are unsynchronized. A post processing algorithm based on Bayesian smoothing is proposed to improve the tracking accuracy, and an offline synchronization algorithm is proposed to correct the time offset between IMU and GNSS measurements. The performance of the proposed algorithms is validated experimentally on a vehicle. It is shown that the tracking accuracy is improved significantly over conventional algorithms.

KEYWORDS: RTK, IMU, Sensor Fusion, vehicle tracking, Post Processing

1. INTRODUCTION

Intelligent transportation system (ITS) improve the efficiency and safety of the transport networks significantly, and GNSS plays an important role in providing positioning information

in ITS. With the recent technological advancements, GNSS receivers can produce positioning results with centimetre-level accuracy. However, a major challenge associated with GNSS is that the positioning accuracy is compromised if the receiver is not in an open-sky environment, e.g., in urban canyons or the shade of trees. For instance, the operation mode of a RTK GNSS receiver switches quickly from fixed to float when it moves into the shade of trees, and it needs more than one minute to regain fixed mode after the receiver returns into an open-sky environment (Morales *et al.*, 2007).

Multi-sensor data fusion (Smith *et al.*, 2006) is a promising technique to improve the performance of GNSS systems in terms of positioning accuracy and integrity. Particularly, IMU has been widely used to complement GNSS receivers (Crassidis 2006 and Grewal *et al.*, 2007), and sensor fusion algorithms based on a Kalman filter have been developed for both highly sensitive IMU sensors (Savage 2000) and low cost ones (Shin 2005). In addition, the GNSS measurements are fused with both IMU measurements and ranges between vehicles in (Wang *et al.*, 2016) to improve the positioning accuracy.

This paper studies the fusion of RTK GNSS receiver and IMU, which offers high tracking accuracy for vehicles travelling in urban canyons or tree shades. Specific focus is placed on the case where the GNSS measurements and IMU measurements are unsynchronized, i.e., there is an unknown time offset between GNSS position measurements and IMU readings. This situation arises when the tracking system is built with GNSS receiver and IMU that operate independently. For example, both the GNSS receiver and IMU are commercial-off-the-shelf (COTS) devices, each generates measurement outputs at a certain rate according to its own clock. The contributions of this paper are as follows:

- A post processing sensor fusion algorithm based on Bayesian smoothing is proposed to improve the tracking accuracy.
- An offline synchronization algorithm is proposed to correct the time offset between IMU and GNSS readings.
- The performance of the proposed algorithms is validated experimentally on a vehicle. It is shown that the tracking accuracy is improved significantly over conventional algorithms.

The remainder of this paper is organized as follows. Section 2 describes the structure of the vehicle tracking system, including the measurement model of the GNSS receiver and IMU. The proposed algorithms for sensor fusion and synchronization are described in Section 3. Section 4 presents the experimental results. Section 5 concludes the paper.

2. System Structure

Figure 1 shows the structure of the vehicle tracking system considered in this paper, which comprises a RTK GNSS receiver and an IMU. The position information provided by the GNSS receiver is fused with the measurements of the IMU to improve the tracking accuracy. This paper is focused particularly on obtaining an accurate estimate of the vehicle trajectory, without any requirement on the timeliness of the fusion algorithm.

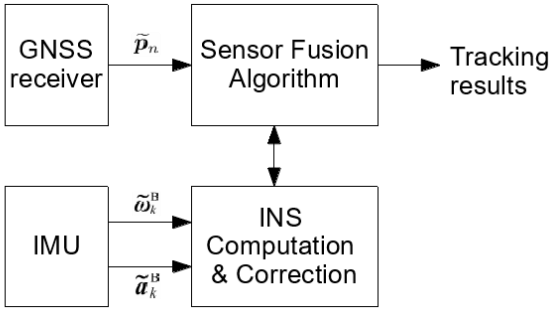

Figure 1 – Structure of the vehicle tracking system.

2.1 RTK GNSS receiver

The GNSS receiver used in the system was a SwiftNav "Piksi" RTK GPS development kit, which operates at GPS L1/L2 frequencies and consists of a RTK base station and a rover unit. Both units are equipped with radios for RTK correction transmissions.

The GNSS receiver provides positional information at 10 Hz update rate. Denote the measured position at time step n as

$$\tilde{\boldsymbol{p}}_n = \boldsymbol{p}_n + \boldsymbol{z}_n, \tag{1}$$

where $\boldsymbol{p}_n$ and $\boldsymbol{z}_n$ denote the true location of vehicle and the measurement error, respectively. The positioning accuracy of the chosen GNSS receiver is about 2cm in RTK fixed mode. However, it switches to float mode quickly if the vehicle is under tree foliage or in urban canyons, in which case the accuracy degrades to 1 – 2m. In addition, it needs more than one minute for the receiver to regain fixed mode after the vehicle gets back into clear-sky conditions, which significantly compromises the reliability of the tracking results.

2.2 IMU sensor

An ADIS16488 MEMS IMU was used in the system. The sensor is attached to a motherboard which consists of a microprocessor and a field programmable logic array (FPGA) for configuring the IMU and retrieving measurement data. The maximum output rate of the IMU is 2460Hz. At each time step k, the outputs of the IMU is denoted by

$$\tilde{\boldsymbol{\omega}}_k^B = \boldsymbol{\omega}_k^B + \boldsymbol{b}_{\omega,k}^B + \boldsymbol{z}_{\omega,k}, \tag{2}$$

$$\tilde{\boldsymbol{a}}_k^B = \boldsymbol{a}_k^B + \boldsymbol{b}_{a,k}^B + \boldsymbol{z}_{a,k}, \tag{3}$$

where $\tilde{\boldsymbol{\omega}}_k^B$ and $\tilde{\boldsymbol{a}}_k^B$ are the measured angular rate and acceleration, respectively, while $\boldsymbol{\omega}_k^B$ and $\boldsymbol{a}_k^B$ are the true angular rate and acceleration, respectively. $\boldsymbol{z}_{\omega,k}$ and $\boldsymbol{z}_{a,k}$ denote the measurement error. $\boldsymbol{b}_{\omega,k}^B$ and $\boldsymbol{b}_{a,k}^B$ denote the measurement bias, which are modelled by random walk processes as below

$$\boldsymbol{b}_{\omega,k+1}^B = \boldsymbol{b}_{\omega,k}^B + \boldsymbol{\eta}_{\omega,k}, \tag{4}$$

$$\boldsymbol{b}_{a,k+1}^B = \boldsymbol{b}_{a,k}^B + \boldsymbol{\eta}_{a,k}, \tag{5}$$

where $\boldsymbol{\eta}_{\omega,k}$ and $\boldsymbol{\eta}_{a,k}$ are random noises that govern the respective random walk processes.

2.3 Synchronization of GNSS and IMU measurements

The GNSS and IMU measurements are recorded along with time stamps indicating the time that each measurement was taken. Denote the time stamp associated with each position measurement $\widetilde{\boldsymbol{p}}_n$ by t_n^{GNSS}, where the superscript $^{\text{GNSS}}$ indicates that the time stamp is recorded based on the clock in the GNSS receiver. Similarly, denote the time stamp associated with each IMU measurement ($\widetilde{\boldsymbol{\omega}}_k^B$ and $\widetilde{\boldsymbol{a}}_k^B$) as t_k^{IMU}, where the superscript $^{\text{IMU}}$ indicates that the time stamp is recorded based on the clock in the IMU.

The GNSS and IMU measurements can be synchronized based on t_n^{GNSS} and t_k^{IMU} under the following conditions:

- Both of the time stamps are accurate, e.g., both are precise Coordinated Universal Time (UTC).
- The clock of the GNSS receiver and that of the IMU are synchronized, e.g., the GNSS receiver and IMU are controlled by the same microprocessor/FPGA.

Neither of the above conditions is meet in the considered system, since the GNSS receiver and the IMU are two independent devices. There is inevitably an offset between the two clocks, which needs to be addressed in the sensor fusion algorithm due to the high speed of the vehicle. For example, a clock offset of 0.5 second between the GNSS receiver and IMU can cause a positional offset of up to 7 meter for a vehicle travelling at 50 km/h, which severely degrades the accuracy of the trajectory estimated by the sensor fusion algorithm.

Define the clock offset between the GNSS receiver and the IMU as t_{Ofst}, which is the adjustment that should be applied to t_n^{GNSS} so that the resulting time stamp is in the same clock scale as t_k^{IMU}. Specifically, a position measurement $\widetilde{\boldsymbol{p}}_n$ is considered to be obtained at the same time as IMU outputs $\widetilde{\boldsymbol{\omega}}_k^B$ and $\widetilde{\boldsymbol{a}}_k^B$ if [1]

$$t_k^{\text{IMU}} \approx t_n^{\text{GNSS}} - t_{\text{Ofst}}. \tag{6}$$

In this paper, t_{Ofst} is estimated and corrected in the sensor fusion algorithm, as will be shown in the following sections.

Note that the problem of unsynchronized measurements does not arise in holistically designed tracking systems where the GNSS receiver and IMU are controlled by the same microprocessor/FPGA. However, it can arise if one tries to evaluate the performance of a sensor fusion algorithm under different combinations of GNSS receivers and IMUs, in which case it is more convenient to run the GNSS receiver and IMU independently (e.g., using COTS development kit) instead of designing a hardware platform for each possible combination.

3. Sensor Fusion with Unsynchronized GNSS and IMU Measurements

This section presents the sensor fusion algorithm for estimating the trajectory of a vehicle with unsynchronized GNSS and IMU measurements. The conventional fusion algorithm based on a Kalman Filter (KF) is first briefly introduced, followed by the proposed post-processing fusion

[1] Clock skew is not considered in this paper since it has negligible impact on the synchronization. For typical crystal oscillators with a frequency stability in the order of 1ppm, it takes 10000 seconds (over two hours) for t_{Ofst} to drift 10 milisecond (which corresponds to a positional offset of 14 cm for a vehicle travelling at 50 km/h). Typical experiments rarely exceed two hours. For the same reason, the clock offset can be considered as invariant during the experiment.

algorithm based on Bayesian smoothing. The algorithm for estimating the clock offset between GNSS receiver and IMU is described subsequently.

3.1 KF-based sensor fusion

The position of the vehicle is computed in an Inertial Navigation System (INS) using the IMU readings and refined using range measurements. Specifically, the attitude, velocity and position of the vehicle is predicted using the IMU readings, following the definitions and procedures in Appendix A. A KF is employed to track and correct the error state of the INS defined as $\delta \boldsymbol{x}_k = \left[\delta \boldsymbol{\psi}_k^T,\ \left(\delta \boldsymbol{v}_k^{\mathrm{N}}\right)^T, \left(\delta \boldsymbol{r}_k^{\mathrm{N}}\right)^T, \left(\delta \boldsymbol{b}_{\omega,k}^{\mathrm{B}}\right)^T, \left(\delta \boldsymbol{b}_{a,k}^{\mathrm{B}}\right)^T \right]^T$, where $\delta \boldsymbol{\psi}_k^T$, $\delta \boldsymbol{v}_k^{\mathrm{N}}$, $\delta \boldsymbol{r}_k^{\mathrm{N}}$, $\delta \boldsymbol{b}_{\omega,k}^{\mathrm{B}}$, and $\delta \boldsymbol{b}_{a,k}^{\mathrm{B}}$ denote the errors in the attitude, velocity, position, gyroscope bias, and accelerometer bias, respectively, with the detailed definition given in (31). The state transition model of $\delta \boldsymbol{x}_k$ is given by

$$\delta \boldsymbol{x}_k = \boldsymbol{A}_k \delta \boldsymbol{x}_{k-1} + \boldsymbol{B}_k \boldsymbol{w}_k, \tag{7}$$

where $\boldsymbol{A}_k$, $\boldsymbol{B}_k$, and $\boldsymbol{w}_k$ are defined in (33), (34), and (35) respectively in Appendix A-3.

If a position measurement $\tilde{\boldsymbol{p}}_n$ is available at time step k (i.e., (6) is satisfied), the KF is updated according to the following observation model

$$\boldsymbol{y}_k = \boldsymbol{H}_k \delta \boldsymbol{x}_k + \boldsymbol{z}_k, \tag{8}$$

where

$$\boldsymbol{H}_k = [\boldsymbol{0}_{3\times 6} \quad \boldsymbol{I}_3 \quad \boldsymbol{0}_{3\times 6}], \tag{9}$$

$$\boldsymbol{y}_k = \hat{\boldsymbol{r}}_k^{\mathrm{N}} - \tilde{\boldsymbol{p}}_n, \tag{10}$$

with $\hat{\boldsymbol{r}}_k^{\mathrm{N}}$ denoting the predicted vehicle location in the INS. Note that loosely couple fusion is employed in this paper because we consider a system where the GNSS receiver and IMU operate independently (e.g., a prototype system with COTS GNSS and IMU modules), as is described in Section 1.

3.2 Sensor fusion based on Bayesian smoothing

The sensor fusion algorithm described in Section 3.1 can be extended by replacing the KF with a Bayesian smoother, which significantly improves the tracking accuracy by estimating the vehicle position based on both the past and future measurements. This section presents a post processing sensor fusion algorithm based on the Rauch-Tung-Striebel (RTS) smoother. The algorithm is described in Algorithm 1, where it is assumed that the clock offset t_{Ofst} is given. The algorithm for estimating t_{Ofst} will be presented in Section 3.3.

Algorithm 1: Post processing sensor fusion for vehicle tracking

Input: GNSS position measurement $\widetilde{\boldsymbol{p}}_n$ and the corresponding time stamp t_n^{GNSS}; IMU measurements $\widetilde{\boldsymbol{\omega}}_k^B$, $\widetilde{\boldsymbol{a}}_k^B$ and the corresponding time stamp t_k^{IMU}; clock offset between the GNSS receiver and the IMU t_{Ofst}; initial orientation, velocity, position of the vehicle; initial biases of IMU sensors; initial covariance matrix of $\delta\boldsymbol{x}_k$ denoted as $\boldsymbol{P}_{0|0}$.

A) For $k = 1, \ldots, K$ where K is the total number of IMU measurements

1) Predict the orientation, velocity, and position of the vehicle with $\widetilde{\boldsymbol{\omega}}_k^B$ and $\widetilde{\boldsymbol{a}}_k^B$ according to (22)-(30).
2) KF prediction, set

$$\boldsymbol{P}_{k|k-1} = \boldsymbol{A}_k \boldsymbol{P}_{k-1|k-1} \boldsymbol{A}_k^T + \boldsymbol{B}_k \boldsymbol{Q}_w \boldsymbol{B}_k^T, \tag{11}$$

where $\boldsymbol{Q}_w \triangleq E[\boldsymbol{w}_k \boldsymbol{w}_k^T]$.

3) KF update:

If $\exists n,\ \left| t_k^{\text{IMU}} + t_{\text{Ofst}} - t_n^{\text{GNSS}} \right| < \frac{\Delta t}{2}$, set

$$\boldsymbol{S}_k = \boldsymbol{H}_k \boldsymbol{P}_{k-1|k-1} \boldsymbol{H}_k^T + \boldsymbol{R}_k, \tag{12}$$

$$\boldsymbol{K}_k = \boldsymbol{P}_{k-1|k-1} \boldsymbol{H}_k^T \boldsymbol{S}_k^{-1}, \tag{13}$$

$$\delta\boldsymbol{x}_{k|k} = \boldsymbol{K}_k \boldsymbol{y}_k, \tag{14}$$

$$\boldsymbol{P}_{k|k} = (\boldsymbol{I} - \boldsymbol{K}_k \boldsymbol{H}_k) \boldsymbol{P}_{k|k-1}, \tag{15}$$

where $\boldsymbol{y}_k$ and $\boldsymbol{H}_k$ are defined as in (8), $\boldsymbol{R}_k$ is the covariance matrix of the measurement error $\boldsymbol{z}_k$ in (8).

Else, set $\delta\boldsymbol{x}_{k|k} = \boldsymbol{0}$, $\boldsymbol{P}_{k|k} = \boldsymbol{P}_{k|k-1}$.

4) Save the INS states.
5) Update the INS states with $\delta\boldsymbol{x}_{k|k}$ according to (31)-(32).

B) For $k = K - 1, \ldots, 0$:

1) Set:

$$\boldsymbol{C}_k = \boldsymbol{P}_{k|k} \boldsymbol{A}_{k+1}^T \boldsymbol{P}_{k+1|k}^{-1}, \tag{16}$$

$$\delta\boldsymbol{x}_{k|K} = \delta\boldsymbol{x}_{k|k} + \boldsymbol{C}_k \delta\boldsymbol{x}_{k+1|K}, \tag{17}$$

$$\boldsymbol{P}_{k|K} = \boldsymbol{P}_{k|k} + \boldsymbol{C}_k \left(\boldsymbol{P}_{k+1|K} - \boldsymbol{P}_{k+1|k} \right) \boldsymbol{C}_k^T. \tag{18}$$

2) Update the saved INS states with $\delta\boldsymbol{x}_{k|K}$ according to (31)-(32).

Output: Estimated trajectory of the vehicle $\{\hat{\boldsymbol{r}}_k^N\}_{k=1}^K$.

3.3 Clock offset estimation

This section presents the proposed algorithm for estimating t_{Ofst}, which is critical to the synchronization of GNSS and IMU measurements as is described in Section 2.3 and Algorithm 1. The algorithm is based on the fact that the vehicle trajectory estimated using Algorithm 1 deviates from the positions measured by the GNSS receiver if t_{Ofst} is assigned an incorrect value, which is due to the inconsistency between IMU readings and GNSS position measurements.

Define the root means square (RMS) difference between the GNSS position measurements and the trajectory obtained using sensor fusion as

$$e = \sqrt{\frac{\sum_n \left(\hat{\boldsymbol{r}}_{k_n}^N - \tilde{\boldsymbol{p}}_n\right)^2}{\sum_n 1}}, \tag{19}$$

where

$$k_n = \arg\min_k \left| t_k^{\mathrm{IMU}} + t_{\mathrm{Ofst}} - t_n^{\mathrm{GNSS}} \right|. \tag{20}$$

Since e is minimized if t_{Ofst} is assigned the correct value, one can estimate t_{Ofst} using a bisection searching algorithm as described in Algorithm 2.

Algorithm 2 Estimate the clock offset between GNSS receiver and IMU

Input: GNSS position measurement $\tilde{\boldsymbol{p}}_n$ and the corresponding time stamp t_n^{GNSS}; IMU measurements $\tilde{\boldsymbol{\omega}}_k^B$, $\tilde{\boldsymbol{a}}_k^B$ and the corresponding time stamp t_k^{IMU}; initial orientation, velocity, position of the vehicle; initial biases of IMU sensors; initial covariance matrix of $\delta \boldsymbol{x}_k$ denoted as $\boldsymbol{P}_{0|0}$.

Initialization: Set $t_{\mathrm{Ofst}}^{\max} = t_{\max\_\mathrm{abs}}$, $t_{\mathrm{Ofst}}^{\min} = -t_{\max\_\mathrm{abs}}$, where $t_{\max\_\mathrm{abs}}$ denote the maximum possible value of $|t_{\mathrm{Ofst}}|$.

While $t_{\mathrm{Ofst}}^{\max} - t_{\mathrm{Ofst}}^{\min} > \epsilon$:

1) Set
$$\hat{t}_{\mathrm{Ofst}} = \frac{t_{\mathrm{Ofst}}^{\max} + t_{\mathrm{Ofst}}^{\min}}{2} \tag{21}$$
2) Apply Algorithm 1 with $t_{\mathrm{Ofst}}^{+} = \hat{t}_{\mathrm{Ofst}} + \xi$, where ξ is a small value. Denote the resulting trajectory as $\left\{\hat{\boldsymbol{r}}_{k,+}^N\right\}_{k=1}^K$.
3) Evaluate the discrepancy between $\left\{\hat{\boldsymbol{r}}_{k,+}^N\right\}_{k=1}^K$ and the GNSS position measurements according to (19), denoting the result as e_+.
4) Apply Algorithm 1 with $t_{\mathrm{Ofst}}^{+} = \hat{t}_{\mathrm{Ofst}} - \xi$. Denote the resulting trajectory as $\left\{\hat{\boldsymbol{r}}_{k,-}^N\right\}_{k=1}^K$.
5) Evaluate the discrepancy between $\left\{\hat{\boldsymbol{r}}_{k,-}^N\right\}_{k=1}^K$ and the GNSS position measurements according to (19), denoting the result as e_-.
6) If $e_+ > e_-$, set $t_{\mathrm{Ofst}}^{\max} = \hat{t}_{\mathrm{Ofst}}$; otherwise set $t_{\mathrm{Ofst}}^{\min} = \hat{t}_{\mathrm{Ofst}}$.

Output: Estimated clock offset $\hat{t}_{\mathrm{Ofst}}$.

4. Experimental Results

This section presents the performance of the proposed algorithms evaluated experimentally.

4.1 Experiment setup

The experiments presented in this paper were conducted in Marsfield, NSW, Australia. The base station unit of the RTK GNSS development kit was placed at a location with known coordinates. The RTK correction was sent to the rover unit via a 2.4GHz radio link. The rover unit was mounted on the roof of a car using a magnetic base, as is shown in Figure 2. The IMU was placed inside the car against the roof underneath the GNSS antenna, so that the lever-arm

effect is minimized. Figure 3 shows a photo of the IMU used in the experiment. The GNSS and IMU measurements were logged with a laptop for post-processing.

Figure 2 – Rover unit mounted on the roof of a car, with the GNSS antenna placed at the centre. The IMU was inside the car and not shown in the figure.

Figure 3 – ADIS16488 MEMS IMU used in the experiment.

The following algorithms were used to track the vehicle:

- **KF-Fusion**: The KF-based sensor fusion algorithm as described in Section 3.1, where the clock offset t_{Ofst} is assumed to be 0.
- **RTS-Fusion**: The post processing sensor fusion algorithm based on Bayesian smoothing as described in Algorithm 1, where the clock offset t_{Ofst} is assumed to be 0.
- **KF-Fusion-Sync**: The KF-based sensor fusion algorithm as described in Section 3.1, with t_{Ofst} estimated using Algorithm 2.
- **RTS-Fusion-Sync**: The post processing algorithm described in Algorithm 1, with t_{Ofst} estimated using Algorithm 2.

4.2 Vehicle tracking results

The vehicle was driven at about 45km/h in a street that is partly covered by tree leaves. Figure 4 shows the vehicle positions measured by the RTK GNSS receiver, where blue dots and red dots indicate RTK fixed mode and float mode, respectively. It can be seen that there is a significant positioning errors in the bottom right corner.

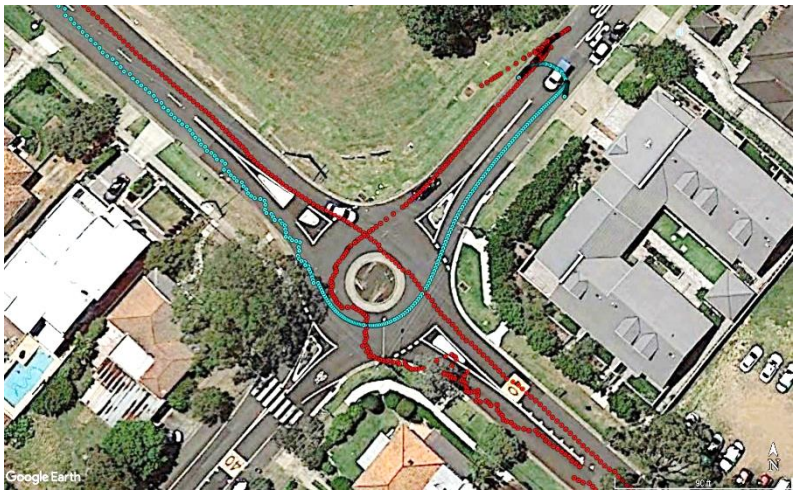

Figure 4 – Vehicle position measured by the RTK GNSS receiver. Blue dots and red dots indicate that the receiver was in RTK fixed mode and floated mode, respectively.

Figure 5 - Figure 8 shows the vehicle positions obtained using the considered sensor fusion algorithms. Comparing Figure 4 with Figure 5 - Figure 8, it can be seen that the tracking accuracy is significantly improved by fusing with IMU readings, particularly for the bottom-right corner where GNSS measurements exhibit large errors. However, part of the trajectory estimated using KF-Fusion is on the wrong side of the road, as is shown in the top-left corner of Figure 5. This is due to the uncorrected clock offset between GNSS receiver and IMU (note that there is no bias in the GNSS position measurements, as can be seen in Figure 5). The accuracy is improved by using Bayesian smoothing in RTS-Fusion, as is shown in Figure 6. In comparison, the accuracy achieved by KF-Fusion-Sync and RTS-Fusion-Sync as shown in Figure 7 and Figure 8 are significantly improved, which is because the GNSS and IMU measurements are synchronized using the estimated t_{Ofst}.

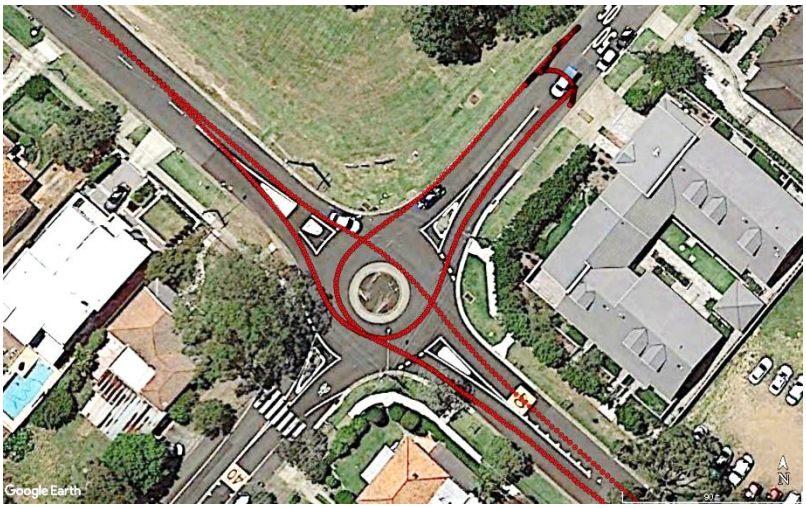

Figure 5 – Vehicle positions obtained using the KF-Fusion algorithm.

Figure 6 – Vehicle positions obtained using the RTS-Fusion algorithm.

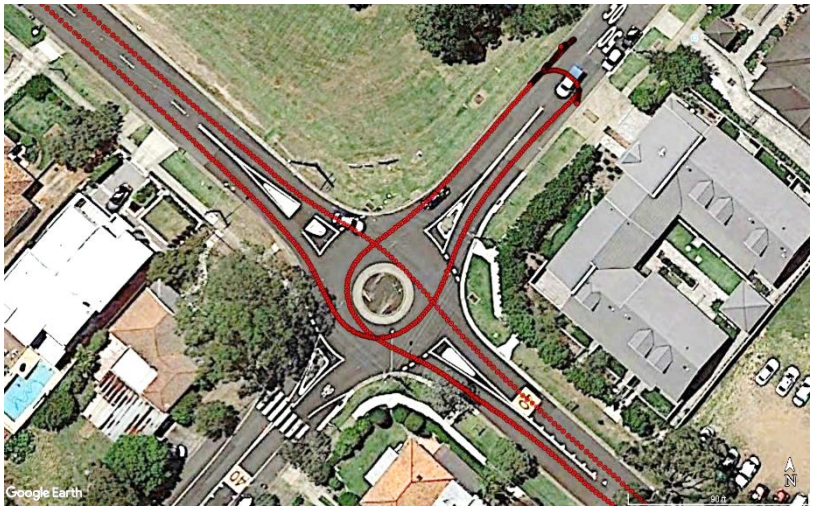

Figure 7 – Vehicle positions obtained using the KF-Fusion-Sync algorithm.

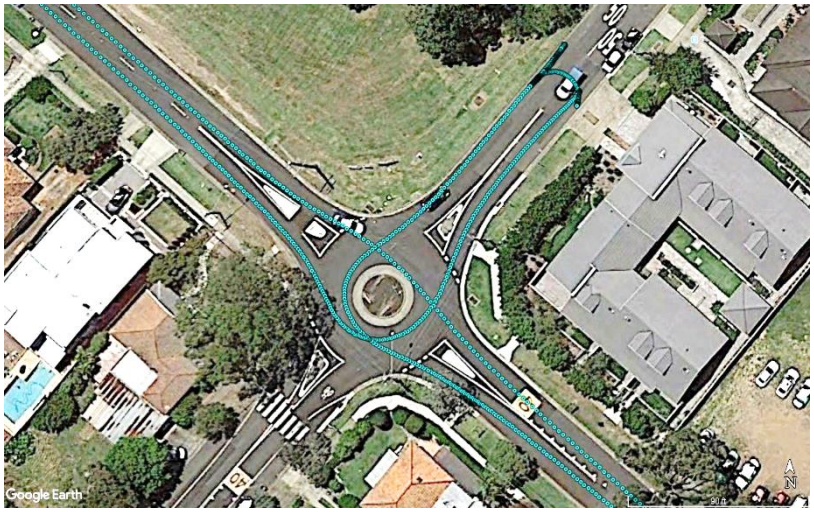

Figure 8 – Vehicle position obtained using the RTS-Fusion-Sync algorithm.

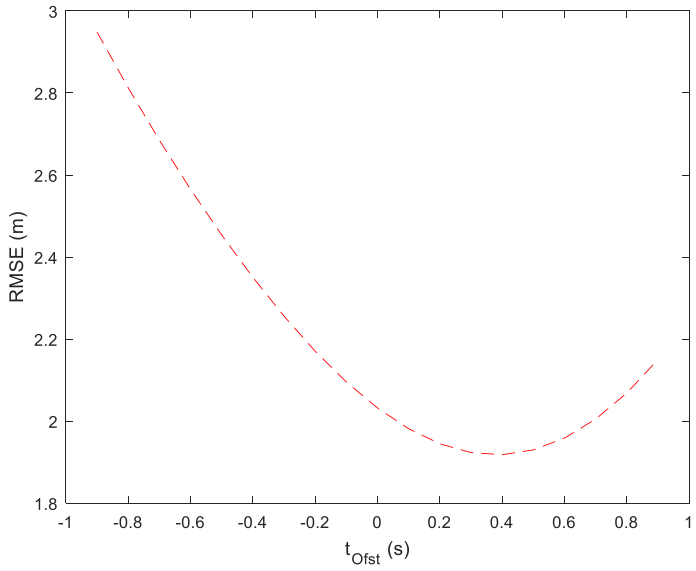

Figure 9 – Relationship between the RMS trajectory discrepancy defined in (19) and $\boldsymbol{t_{\mathrm{Ofst}}}$.

Figure 9 shows the RMS trajectory discrepancy defined in (19) under different t_{Ofst}. It can be seen that the discrepancy is minimized when $t_{\mathrm{Ofst}} = 0.4$, which indicates that the clock offset between the GNSS receiver and the IMU is 0.4 second. The tracking accuracy is significantly improved by taking this offset into account, as is shown in Figure 5 - Figure 8.

The effect of the clock offset is also visible in a different part of the trajectory where the vehicle made a three-point turn. Figure 10-12 show the GNSS position measurement, the trajectory estimated with RTS-Fusion, and that estimated with RTS-Fusion-Sync, respectively. It can be seen from Figure 11 that the trajectory is distorted if the clock offset is not considered. On the other hand, the trajectory estimated by RTS-Fusion-Sync in Figure 12 is consistent with the trajectory of a three-point turn.

Figure 10 - Vehicle position measured by the RTK GNSS receiver when the vehicle was making a three-point turn.

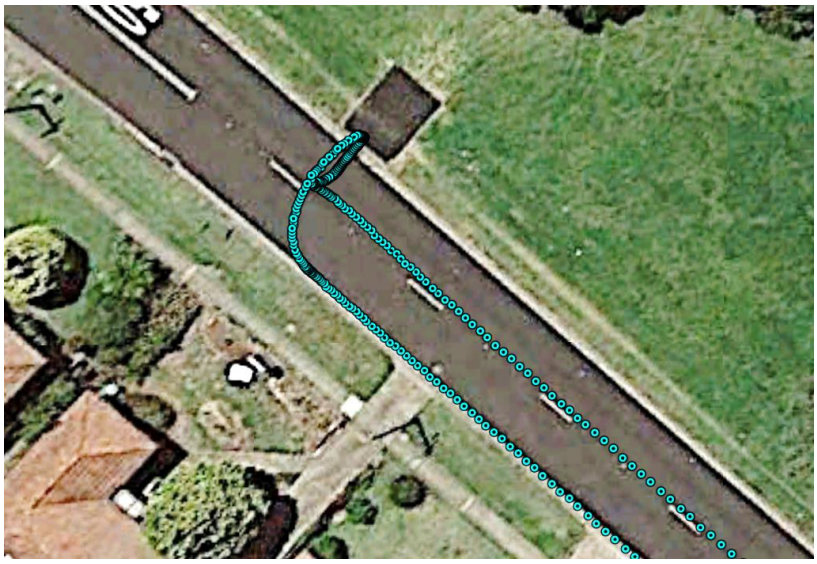

Figure 11 – Vehicle trajectory obtained using the RTS-Fusion algorithm for the part of trajectory shown in Figure 10. The trajectory is distorted due to uncompensated clock offset.

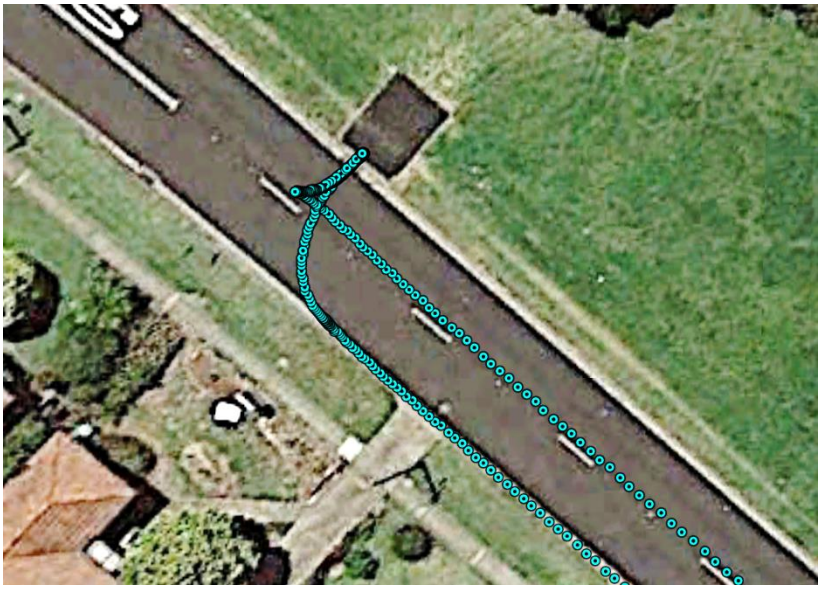

Figure 12 - Vehicle trajectory obtained using the RTS-Fusion-Sync algorithm for the part of trajectory shown in Figure 10. The accuracy is significantly improved by taking the clock offset into account. The trajectory is consistent with that shown in Figure 10, and the pattern of three-point turn is clearly visible.

4.3 Walking test

Since no knowledge is available about the true vehicle positions, the results presented in Section 4.2 can only be evaluated qualitatively by comparing the estimated trajectory against the lanes in the road. To evaluate the performance of the proposed algorithms quantitatively, a walking test was conducted at the Marsfield site of CSIRO. The rover unit and IMU was moved along straight lines which were surveyed and used as the ground truth trajectory.

Figure 13 shows the tracking results for the walking test. The GNSS receiver was in RTK fixed mode most of the time, except for a short period of float mode when it was under tree foliage (the top left corner of the diagram). The clock offset between GNSS receiver and IMU was neglected during processing due to the low speed of walking. Therefore the results of KF-Fusion is almost identical to that of KF-Fusion-Sync (the same for RTS-Fusion and RTS-

Fusion-Sync). It can be seen in the figure that the tracking accuracy is significantly improved during the period of RTK float mode by employing RTS-Fusion.

Figure 14 shows the cumulative distribution function (CDF) of the positioning errors during the period of RTK float mode. Specifically, the positioning error is characterized by the deviation of the estimated positions from the straight line that is aligned with P12-P19 in Figure 13. It can be seen that the performance of RTS-Fusion is significantly higher than that of KF-Fusion, with a maximum positioning error of about 20 cm.

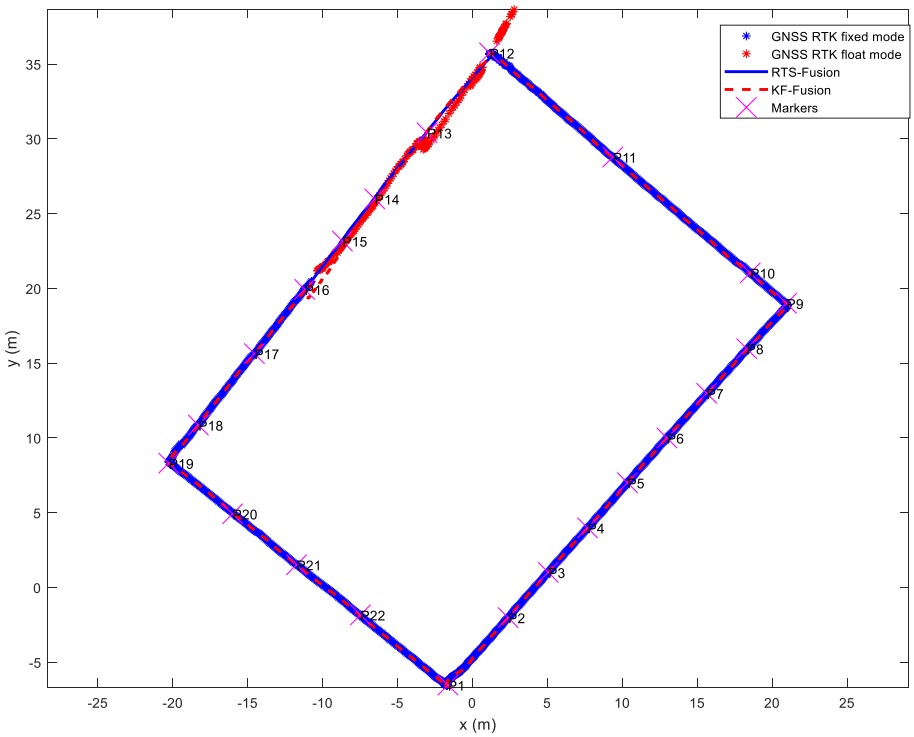

Figure 13 – Tracking result in the walking test. The red crosses indicate the markers along the straight lines whose locations were surveyed.

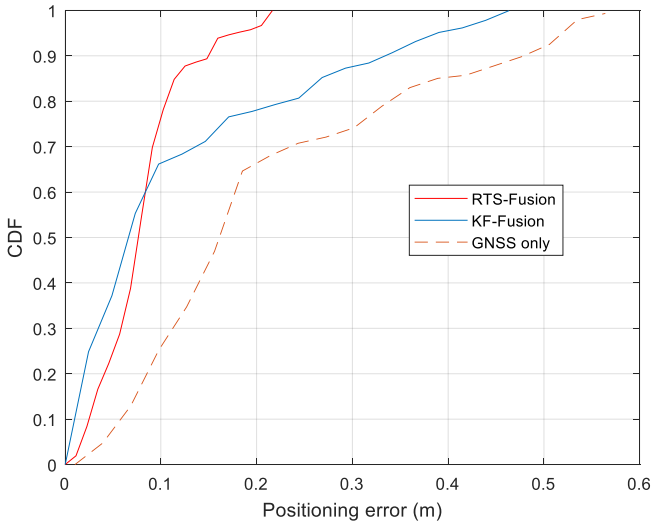

Figure 14 – CDF of positioning error in the walking test.

Conclusion

RTK GNSS receiver augmented with high quality IMU can provide highly accurate tracking results for vehicles. This paper studies the fusion of GNSS and IMU measurements, with a specific focus on the case where the two type of sensors are not clock synchronized. A post processing algorithm based on Bayesian smoothing is proposed to improve the tracking accuracy, and an offline synchronization algorithm is proposed to correct the time offset between IMU and GNSS measurements. The performance of the proposed algorithms is validated experimentally. It is shown that the tracking accuracy is improved significantly over conventional algorithms.

APPENDIX A

A.1 Basic Definitions

The following Cartesian coordinate frames are used in this paper:

- **B-Frame**: Body frame that is fixed to the IMU, with axes parallel to those of the triaxial gyroscope and accelerometer.
- **N-Frame**: North-East-Down (NED) frame with the X, Y, and Z axis pointing north, east, and down respectively.

Vectors described in B-Frame and N-Frame are denoted with superscripts $^{\mathrm{B}}$ and $^{\mathrm{N}}$, respectively. In addition, the attitude of the B-Frame with respect to the N-Frame is represented with a Direction Cosine Matrix (DCM) $C_{\mathrm{B}}^{\mathrm{N}}$.

A.2 INS State Prediction

To predict the states of the vehicle using IMU readings, the bias in $\widetilde{\boldsymbol{\omega}}_k^B$ is first corrected by

$$\widehat{\boldsymbol{\omega}}_k^B = \widetilde{\boldsymbol{\omega}}_k^B - \widehat{\boldsymbol{b}}_{\omega,k}^B, \tag{22}$$

where $\widehat{\boldsymbol{b}}_{\omega,k}^B$ is the estimated bias in the rate gyro measurement. Integrating $\widehat{\boldsymbol{\omega}}_k^B$ between time step $k-1$ and k results in a rotation vector (Savage 2000) for computing the attitude. Specifically,

$$\phi_k = \int_{t_{k-1}^{IMU}}^{t_k^{IMU}} \widehat{\boldsymbol{\omega}}_k^B \, dt \approx \widehat{\boldsymbol{\omega}}_k^B \Delta t, \tag{23}$$

where $\Delta t \triangleq t_k^{IMU} - t_{k-1}^{IMU}$. The attitude is then computed by

$$\hat{C}_{\mathrm{B},k}^{\mathrm{N}} = \hat{C}_{\mathrm{B},k}^{\mathrm{N}} C(\phi_k), \tag{24}$$

where $C(\phi)$ denotes the DCM corresponding to a rotation vector ϕ, which is given by (Savage 2000)

$$C(\phi) = \boldsymbol{I} + \frac{\sin|\phi|}{|\phi|}(\phi\times) + \frac{1-\cos|\phi|}{|\phi|^2}(\phi\times)(\phi\times). \tag{25}$$

Note that $(\phi\times)$ in the above equation denotes the skew symmetric cross-product matrix of a vector $\phi = [\phi_1, \phi_2, \phi_3]^T$ as below

$$(\phi\times)=\begin{bmatrix}0 & -\phi_3 & \phi_2\\ \phi_3 & 0 & -\phi_1\\ -\phi_2 & \phi_1 & 0\end{bmatrix}. \tag{26}$$

The measured acceleration is then transformed from B-Frame to N-Frame as follows

$$\widehat{\boldsymbol{a}}_k^{\mathrm{N}}=\hat{C}_{\mathrm{B},k}^{\mathrm{N}}\widehat{\boldsymbol{a}}_k^{B}, \tag{27}$$

where $\widehat{\boldsymbol{a}}_k^{B}$ denotes the B-Frame acceleration after bias correction, i.e.,

$$\widehat{\boldsymbol{a}}_k^{B}=\widetilde{\boldsymbol{a}}_k^{B}-\widehat{\boldsymbol{b}}_{a,k}^{\mathrm{B}}. \tag{28}$$

The velocity and position of the vehicle are then predicted according to

$$\widehat{\boldsymbol{v}}_k^{\mathrm{N}}=\widehat{\boldsymbol{v}}_{k-1}^{\mathrm{N}}+\left(\widehat{\boldsymbol{a}}_k^{\mathrm{N}}+[0,0,G]^T\right)\Delta t, \tag{29}$$

$$\hat{\boldsymbol{r}}_k^{\mathrm{N}}=\hat{\boldsymbol{r}}_{k-1}^{\mathrm{N}}+\hat{\boldsymbol{v}}_k^{\mathrm{N}}\Delta t, \tag{30}$$

where G denotes the gravitational acceleration.

A.3 KF State Transition Model

The state of the KF is defined as

$$\delta\boldsymbol{x}_k=\begin{bmatrix}\delta\boldsymbol{\psi}_k\\ \delta\boldsymbol{v}_k^{\mathrm{N}}\\ \delta\boldsymbol{r}_k^{\mathrm{N}}\\ \delta\boldsymbol{b}_{\omega,k}^{\mathrm{B}}\\ \delta\boldsymbol{b}_{a,k}^{\mathrm{B}}\end{bmatrix}\triangleq\begin{bmatrix}\delta\boldsymbol{\psi}_k\\ \widehat{\boldsymbol{v}}_k^{\mathrm{N}}-\boldsymbol{v}_k^{\mathrm{N}}\\ \hat{\boldsymbol{r}}_k^{\mathrm{N}}-\boldsymbol{r}_k^{\mathrm{N}}\\ \widehat{\boldsymbol{b}}_{\omega,k}^{\mathrm{B}}-\boldsymbol{b}_{\omega,k}^{\mathrm{B}}\\ \widehat{\boldsymbol{b}}_{a,k}^{\mathrm{B}}-\boldsymbol{b}_{a,k}^{\mathrm{B}}\end{bmatrix}, \tag{31}$$

where $\boldsymbol{v}_k^{\mathrm{N}}$ and $\boldsymbol{r}_k^{\mathrm{N}}$ denote the true velocity and position of the vehicle at time step k, respectively. $\delta\boldsymbol{\psi}_k$ is the Psi-angle error characterizing (Savage 2000 and Shin 2005) the attitude error, which is defined as below

$$C_{\mathrm{B},k}^{\mathrm{N}}=C(\delta\boldsymbol{\psi}_k)\hat{C}_{\mathrm{B},k}^{\mathrm{N}}, \tag{32}$$

where $C_{\mathrm{B},k}^{\mathrm{N}}$ denotes the true attitude of the vehicle at time step k, $C(\cdot)$ is defined in (25).

The variables in the error state transition model (7) are given by

$$\boldsymbol{A}_k=\boldsymbol{I}+\begin{bmatrix}\boldsymbol{0} & \boldsymbol{0} & \boldsymbol{0} & \hat{C}_{\mathrm{B},k}^{\mathrm{N}} & \boldsymbol{0}\\ \left(\hat{C}_{\mathrm{B},k}^{\mathrm{N}}\widehat{\boldsymbol{a}}_k^{B}\right)\times & \boldsymbol{0} & \boldsymbol{0} & \boldsymbol{0} & -\hat{C}_{\mathrm{B},k}^{\mathrm{N}}\\ \boldsymbol{0} & \boldsymbol{I} & \boldsymbol{0} & \boldsymbol{0} & \boldsymbol{0}\\ \boldsymbol{0} & \boldsymbol{0} & \boldsymbol{0} & \boldsymbol{0} & \boldsymbol{0}\\ \boldsymbol{0} & \boldsymbol{0} & \boldsymbol{0} & \boldsymbol{0} & \boldsymbol{0}\end{bmatrix}\Delta t, \tag{33}$$

$$\boldsymbol{B}_k=\begin{bmatrix}-\hat{C}_{\mathrm{B},k}^{\mathrm{N}} & \boldsymbol{0} & \boldsymbol{0} & \boldsymbol{0}\\ \boldsymbol{0} & \hat{C}_{\mathrm{B},k}^{\mathrm{N}} & \boldsymbol{0} & \boldsymbol{0}\\ \boldsymbol{0} & \boldsymbol{0} & \boldsymbol{0} & \boldsymbol{0}\\ \boldsymbol{0} & \boldsymbol{0} & \boldsymbol{I} & \boldsymbol{0}\\ \boldsymbol{0} & \boldsymbol{0} & \boldsymbol{0} & \boldsymbol{I}\end{bmatrix}\Delta t, \tag{34}$$

$$\boldsymbol{w}_k = \begin{bmatrix} \boldsymbol{z}_{\omega,k} \\ \boldsymbol{z}_{a,k} \\ \boldsymbol{\eta}_{\omega,k} \\ \boldsymbol{\eta}_{a,k} \end{bmatrix}, \tag{35}$$

where $\hat{C}_{\mathrm{B},k}^{\mathrm{N}}$ and $\widehat{\boldsymbol{a}}_k^B$ are defined in (24) and (28), respectively, the elements in $\boldsymbol{w}_k$ are defined in (2)-(5).

REFERENCES

Crassidis J (2006) Sigma-point Kalman filtering for integrated GPS and inertial navigation, IEEE Transactions on Aerospace and Electronic Systems, 42(2): 750–756

Grewal MS, Weill LR, Andrews AP (2007) Global positioning systems, inertial navigation, and integration, John Wiley & Sons

Grewal MS, Andrews AP (2014) Kalman filtering: Theory and Practice with MATLAB, John Wiley & Sons, 2014.

Morales Y, Tsubouchi T (2007) DGPS, RTK-GPS and StarFire DGPS Performance Under Tree Shading Environments, Proceedings of IEEE International Conference on Integration Technology 2007, Shenzhen, 519-524

Savage P (2000) Strapdown Analytics, Strapdown Associates

Shin EH (2005) Estimation techniques for low-cost inertial navigation, UCGE report, 20219

Smith D, Singh S (2006) Approaches to multi sensor data fusion in target tracking: A survey, IEEE Transactions on Knowledge and Data Engineering, 18(12): 1696–1710

Wang J, Gao Y, Li Z, Meng X, Hancock CM (2016) A Tightly-Coupled GPS/INS/UWB Cooperative Positioning Sensors System Supported by V2I Communication, Sensors (Basel, Switzerland),16(7):944